

Study on the Thermal Sensitivity of Anisotropic Thin Sheets: Application to Hot Bulge Tests

Aboulbaba ELADEB*, **Mohamed Toumi NASRI********, **Nidhal BECHEIKH***, **Nejib GHAZOUANI*******, **Mohammed A. TASHKANDI***

*College of Engineering, Northern Border University, PO Box 1321 Arar, Northern Borders 73222, Saudi Arabia, E-mails: aboulbaba.eladeb@nbu.edu.sa, nidhal.becheikh@nbu.edu.sa, nejib.ghazouani@nbu.edu.sa, mohammed.tashkandi@nbu.edu.sa

**LMPE (LR18ES01), Ecole Nationale Supérieure d'Ingénieurs de Tunis (ENSIT), Université de Tunis, 5 Av. Taha Hussein, Montfleury 1008 Tunis, Tunisia, E-mail: mohamedtoumi.nasri@enib.ucar.tn

***National Engineering School of BIZERTE, University of Carthage, BP66, Menzel Abderrahman University Campus 7035, Bizerte, Tunisia

****Civil Engineering Laboratory, National Engineers School of Tunis (ENIT), University of Tunis El Manar, Tunis 1002, Tunisia

<https://doi.org/10.5755/j02.mech.34214>

1. Introduction

The transformation of mechanical sheets into finished products is of considerable importance in many industries such as mechanical engineering, automotive or aeronautics. The premature tearing of sheet metal during shaping is one of the major problems currently facing the mechanical industry [1-3]. Scientists and industrialists are therefore always looking for the best conditions for which the ability to deform can in turn go to a maximum in order to minimize scrap.

Responsiveness to market demand requires a reduction in the development time of product manufacturing lines. Very short deadlines and requirements in terms of product quality now require manufacturing processes to be well controlled and optimized [4-6]. Today, improvements will mainly come from gains that will be made in the control of manufacturing processes. This implies a realistic, reliable and fast modeling of all the physical phenomena that characterize forming operations such as the behavior of the material, the wear of the tools, and the influence of the parameters of the operation [7-9]. Works have studied the feasibility of increasing the temperature as an approach to solve the problem of ductility of Al 1050 and increasing the strength of the material [10-13]. In addition, the amount of elongation and the level of the forming limit diagram were reduced, but increased at low speeds. Forming limit curves have been used to assess the formability of materials [14, 15, 16].

Hydroforming and all processes for obtaining parts by deformation of metallic materials are processes widely used in mechanical manufacturing and which are constantly advancing technologically to reach new markets [17, 18].

To determine the best forming process, the numerical simulation of the forming processes constitutes a privileged means of investigation [19]. By providing access to quantities that are difficult to access through experience, it improves the understanding of simulated phenomena. In addition, it makes it possible to analyze a process before it is actually implemented. It makes it possible to estimate according to different parameters if a part is or is not shaped [20]. New ideas can thus be tested without mobilizing the production tool.

But numerical simulation is based on mathematical models and laws of behavior which must satisfy the general principles of mechanics and which are physically acceptable. These mathematical models must on the one hand take into account the stresses that the materials undergo during their deformation and take account of all the parameters involved in a process and on the other hand, they must be simple in order to facilitate their identification and their implementation in computer codes [21]. Indeed, the numerical simulation of a shaping process is a complex process during which a large number of physical phenomena are involved. Taking all these phenomena into account, even in a simple way, requires too long a calculation time [22, 23].

To remedy, on the one hand, the long calculation time that a numerical simulation or an optimization procedure can take and, on the other hand, the inadequacy of the mathematical models, tools based on artificial intelligence are being developed. The aim of this work is to develop a method for modeling and optimizing shaping processes coupled with a finite element calculation code.

2. Theory of plasticity for anisotropic material

2.1. Anisotropic material

The quadratic anisotropic yield criterion Hill 48 [24] under plane stress state is used to describe the anisotropic mechanical behavior. The yield function can be written as:

$$\bar{\sigma}^2 = F(\sigma_y - \sigma_z)^2 + G(\sigma_z - \sigma_x)^2 + H(\sigma_x - \sigma_y)^2 + V, \quad (1)$$

where $V = 2L\tau_{yz}^2 + 2M\tau_{zx}^2 + 2N\tau_{xy}^2$.

It assumes the x and y directions as the rolling direction and the transversal to the rolling direction, respectively. Here σ_{xx} and σ_{yy} are the normal stresses along the x -direction (rolling direction) and y -direction (transverse direction); σ_{xy} is the shear stress; F , G , H , and N are material parameters, which can be expressed by Lankford's coefficients:

$$F = \frac{r_0}{r_{90}(r_0 + 1)},$$

$$G = \frac{1}{(r_0 + 1)},$$

$$H = \frac{r_0}{(r_0 + 1)},$$

$$N = \frac{(r_0 + r_{90})(1 + 2r_{45})}{2r_{45}(r_0 + 1)}. \quad (2)$$

The used anisotropic plasticity potential of Hill48 is available in the finite element software ABAQUS and defined by the specified material parameters: R_{11} , R_{22} , R_{33} and R_{12} which are defined by:

$$\begin{cases} F = \frac{1}{2} \left(\frac{1}{R_{22}^2} + \frac{1}{R_{33}^2} - \frac{1}{R_{11}^2} \right) \\ G = \frac{1}{2} \left(\frac{1}{R_{33}^2} + \frac{1}{R_{11}^2} - \frac{1}{R_{22}^2} \right) \\ H = \frac{1}{2} \left(\frac{1}{R_{11}^2} + \frac{1}{R_{22}^2} - \frac{1}{R_{33}^2} \right) \\ N = \frac{3}{2R_{12}^2} \end{cases}. \quad (3)$$

Under plane-stress condition, the effective stress in terms of the principal axial and hoop stress is defined as:

$$\bar{\sigma}^2 = [(G + H)\sigma_1^2 + (F + H)\sigma_2^2 - 2H\sigma_1\sigma_2], \quad (4)$$

where σ_1 and σ_2 are the principal axial and hoop stress, respectively.

The plastic strain increments are given by considering the normality condition, incompressibility condition and the equivalent work definition of effective strain increment $d\bar{\varepsilon}$:

$$\begin{cases} d\varepsilon_1 = [(G + H)\sigma_1 - H\sigma_2] \frac{d\bar{\varepsilon}}{\bar{\sigma}}, \\ d\varepsilon_2 = [(F + H)\sigma_2 - H\sigma_1] \frac{d\bar{\varepsilon}}{\bar{\sigma}}, \\ d\varepsilon_3 = -(d\varepsilon_1 + d\varepsilon_2), \end{cases} \quad (5)$$

where $d\varepsilon_1$, $d\varepsilon_2$ and $d\varepsilon_3$ are the plastic strain incremental components along the principal axial, hoop and thickness directions, respectively.

2.2. Criterion of plastic instability

The problem is based on response variables z_1, z_2, \dots, z_p and an influencing factor x whose multiple regression leads to a relation of the form:

$$x = a_0 + a_1 z_1 + a_2 z_2 + \dots + a_p z_p + \varepsilon. \quad (6)$$

Here $a_0, a_1, a_2, \dots, a_p$ are the coefficients of the regression, ε is an error.

To validate the quality of the regression equation between the influence factor and the response variables, we use the multiple determination coefficient defined by Eq. (7), where SCR and SCT are the squared sums of deviations:

$$R^2 = \frac{SCR}{SCT}. \quad (7)$$

2.3. Identification method

The variation of the principal stress components in terms of the principal hoop stress can be derived as [25].

$$\begin{cases} d\sigma_1 = \frac{d\bar{\varepsilon}}{\bar{\sigma}} [(G + H)\alpha^2 - 2H\alpha + F + H] \sigma_2^2 \\ d\sigma_2 = \frac{d\bar{\varepsilon}}{\bar{\sigma}} [(G - H)\alpha + 2F + H] \sigma_2^2 \end{cases}. \quad (8)$$

Based on Eqs. (6) and (8), the variation of the effective stress is deduced as:

$$d\bar{\sigma} = \bar{\sigma} d\bar{\varepsilon} Y, \quad (9)$$

where: $\alpha = \frac{\sigma_1}{\sigma_2}$,

$$Y = \frac{\alpha [(G + H)\alpha - H]^2 + 2(F + H - \alpha H)(F + \alpha G)}{[(G + H)\alpha^2 - 2H\alpha + F + H]^{3/2}}.$$

Thus, the plastic instability condition in terms of sub-tangent Z for hydroforming process is obtained as (Fig. 1):

$$\frac{1}{Z} = \frac{1}{\bar{\sigma}} \frac{d\bar{\varepsilon}}{\bar{\sigma}} \leq Y. \quad (10)$$

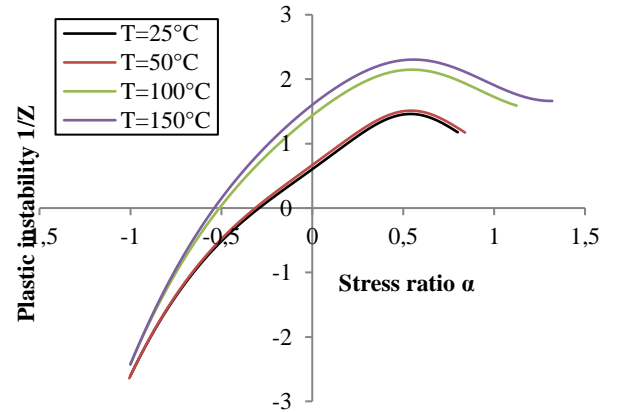


Fig. 1 Plastic instability with different temperature level plastic anisotropy parameters

To obtain forming limit curves in terms of stresses in hydroforming, it is necessary to firstly introduce the principal critical strains ε_1^c and ε_2^c along the axial and hoop direction, respectively.

With the work-hardening law, Eq. (10), can be written as:

$$\bar{\sigma} = K \left[1 - \left(\frac{\bar{\varepsilon} + \varepsilon_s}{\varepsilon_u} \right)^\gamma \right] (\varepsilon_0 + \bar{\varepsilon})^n. \quad (11)$$

Let $\beta = \frac{\varepsilon_1}{\varepsilon_2}$ and assuming the proportional loading, thus the equivalent strain can be described as:

$$\frac{1}{Z} = \frac{1}{\bar{\sigma}} \frac{d\bar{\varepsilon}}{d\sigma} = \frac{n}{\varepsilon_0 + \bar{\varepsilon}} - \frac{\gamma(\varepsilon_s + \bar{\varepsilon})^{\gamma-1}}{\varepsilon_u^\gamma - (\varepsilon_s + \bar{\varepsilon})^\gamma} = \frac{\psi}{\Omega}, \quad (12)$$

$$\bar{\varepsilon} = \left[\frac{(H+F)\varepsilon_1^2 + (G+H)\varepsilon_2^2 + 2H\varepsilon_1\varepsilon_2}{FG+FH+GH} \right]^{1/2} = X\varepsilon_2. \quad (13)$$

Here:

$$X = \left[\frac{(H+F)\beta^2 + 2H\beta + G+H}{FG+FH+GH} \right]^{1/2}, \quad \beta = \frac{\varepsilon_1}{\varepsilon_2}. \quad (14)$$

According to Eqs. (12) and (13), the limit strains based on the plasticity instability yield as:

$$\begin{cases} \varepsilon_1^c = \beta\varepsilon_2^c \\ \varepsilon_2^c = \frac{n}{X} \left[\frac{\Omega}{\psi} - \frac{\varepsilon_0}{n} \right]. \end{cases} \quad (15)$$

From Eq. (4) the limit stress σ_1^c and σ_2^c ; when the bursting failure is occurred, can be obtained as:

$$\begin{cases} \sigma_1^c = \frac{\bar{\sigma}}{\varepsilon} \left[\frac{(F+H)\varepsilon_1^c + H\varepsilon_2^c}{FG+FH+GH} \right] \\ \sigma_2^c = \frac{\bar{\sigma}}{\varepsilon} \left[\frac{(G+H)\varepsilon_2^c + H\varepsilon_1^c}{FG+FH+GH} \right]. \end{cases} \quad (16)$$

3. Experimental set-up

The realization of the experimental tests constitutes a very important stage in the procedure of identification of the parameters of the laws of behaviour. This is a task that is often difficult and costly in terms of raw materials and experimental equipment.

We briefly describe our experimental approach and the material means implemented in our test campaign as well as the various raw experimental results such as the measurement of pressure, temperature, the average speed of deformation as well as the displacements of the height at the pole of the sheet to be shaped and the effect of anisotropy on the behaviour of the sheet is studied.

The device is made up of four sub-assemblies.

- ❖ System for fixing the blanks and clamping the dies: the blank holder is held tight on the clamping system by means of several bolts, a ring is added to the entire periphery of the blank holder so as to eliminate the flow of the material (ensure a better seal between the blank and the die) and thus achieve an embedding, see Fig. 2, a, b and c.

- ❖ Hydraulic system: its role is to provide the power needed to form the blanks (Fig. 2, d).
- ❖ Heating and temperature control system, its role is to convert electrical energy into heat energy and control of the heating temperature of the sheets (Fig. 2, e).
- ❖ Electrical control circuit: ensures the electrical energy supply to the heating system and the hydraulic installation.
- ❖ A protective cover has been designed in tempered glass, it is held by metal supports in order to protect the experimenter against the jets of hot liquid under pressure which may occur during a sudden bursting of the specimens when the fluid pressure reached its maximum value (Fig. 2, f).

In this test the expansion deformations are predominant. The test highlights the importance of the properties of the material for these deformations, and the low importance of the geometric parameters (Fig. 3).

Notations used in the experimental test description: e_0 – initial blank thickness; e – current thickness at the pole; H – height at the pole; D – inner diameter of the die; D' – outside diameter of the die; rc – die fillet diameter; F_S – clamping force; P – Pressure applied to the sheet.

The specimens used are circular blanks with an external diameter of 330 mm and a thickness of 0.6 mm. The active part provided for expansion depends on the auxiliary matrix used. In the case of free expansion tests with a circular die, the active part has a diameter of 200 mm. In the case of an elliptical matrix with the same outer diameter as the previous one, comprising an elliptical recess (small diameter = 102 mm and large diameter = 170 mm).

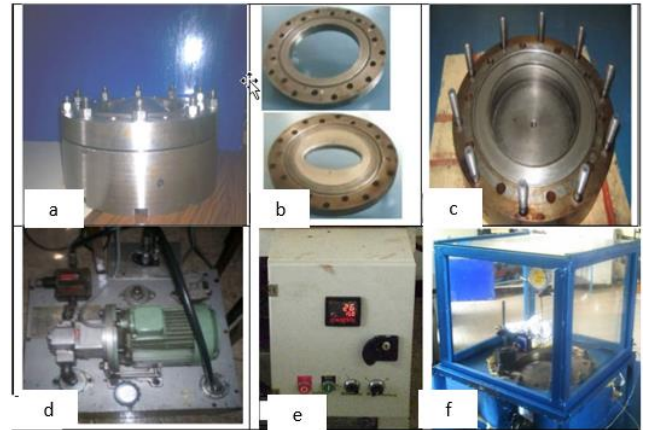


Fig. 2 Hot bulge test equipment

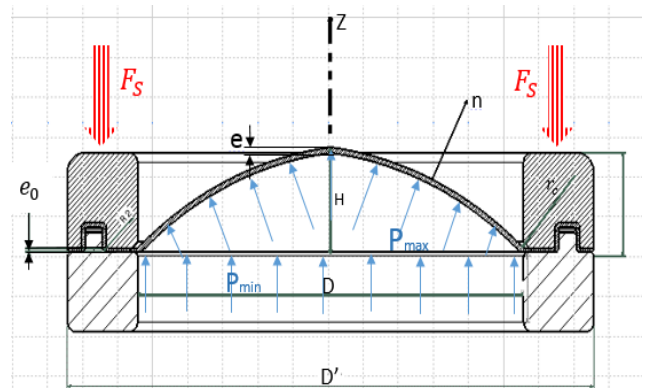


Fig. 3 Principle and configuration of the bulge test

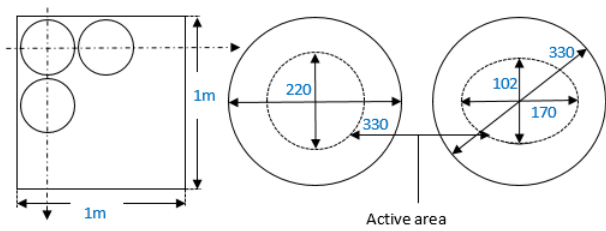


Fig. 4 Cutting sheet metal into a circular shape

The preparation of specimens from a virgin sheet requires precautions responding to the specificities of the test and the geometric shape of the loading device. The preparation steps are shown in Fig. 4.

After the laser cutting operations of the specimens, it was scheduled to print the grids. The shape of the grid chosen is the square 5x5 mm (Fig. 5), the tracing is done using a dedicated printing device and carried out by a specialized company. The grids are drawn on the outer surface of the specimens, so that a pair of sides coincides with the rolling direction of the sheet. The bulge test of the sheet is obtained by applying oil pressure exerted by a manual pump and measured by a pressure sensor. Monitoring of the shape of the blank during the test is obtained by a sensor.

The loading range considered is a function of the nature of the material and the dimensional characteristics of the specimens. The device makes it possible to reach pressures leading to the appearance of localized strictures, this instability is often followed by the appearance of cracks.

Furthermore, for a given pressure applied to the specimen, it will be possible to recover the following measurements at a given point:

- the height at the pole (at each temperature and at each angle of anisotropy),
- the strain,
- the blank thickness.

The type of stress is essentially conditioned by the shape of the matrix and the anisotropy of the material. To take these two parameters into account, we used two types of matrix, one circular and the other elliptical presented in Fig. 6.

The tests are carried out on an instrumented hydraulic inflation cell. It is equipped with two sensors: one for pressure measurement and the other for displacement measurement at the pole.



Fig. 5 Sheet before and after strain of bulge test



a
b
Fig. 6 Dies: a – circular die, b – elliptical

4 Experimental Results and discussion

4.1. Hot forming circular bulge test result

The experimental study carried out provides us with the following measures: the height at the pole as a function of the pressure at different temperatures.

The hydroforming tests were carried out in order to evaluate the hot forming abilities of the material. These tests were carried out at an average strain rate of about 5.10⁻⁴/s and at four temperature levels were taken into consideration (25°C, 100°C, 150°C and 200°C). Fig. 7 presents the pressure/height curves at the pole at different temperature levels. Fig. 8 shows that for the same hydraulic pressure an increase in temperature causes a rise in the height at the pole, this generates an evolution of the maximum joint height with a drop in the maximum pressure because the material becomes more deformable and loses a can their mechanical characteristic at elevated temperatures.

Thus, for a temperature variation of 150°C, the maximum height at bursting undergoes an increase evaluated at around 27% and a decrease in pressure of 21% as shown in Fig. 8.

The height at the pole as a function of the pressure at different average strain rates: Fig. 9 presents the pressure-height curves at the pole relating to this series of tests. We notice that the maximum height at the pole decreases and the maximum pressure increases when the average strain rate increases as shown in Fig. 10.

For an average strain rate variation from 2.5 E-3/s to 5 E-4/s, the maximum bursting height undergoes a

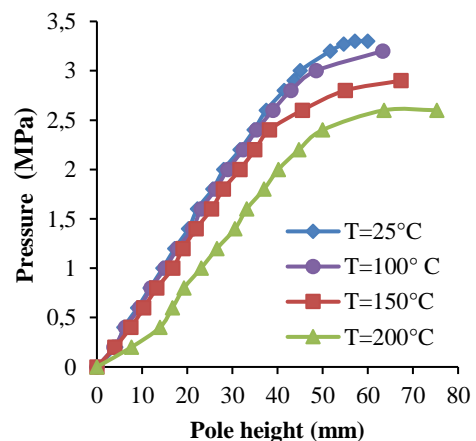


Fig. 7 Pressure as a function of height at the pole: circular matrix (temperature effect)

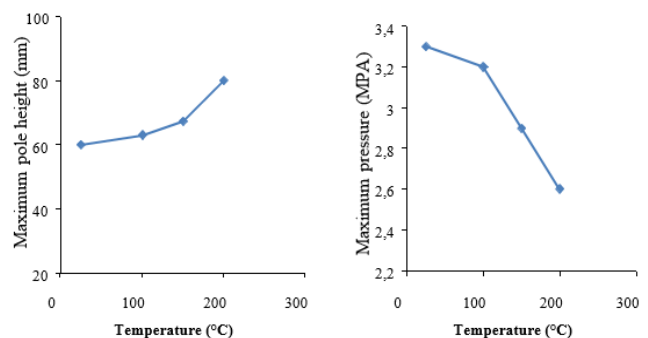


Fig. 8 Maximum pressure and Maximum height at the pole as a function of temperature

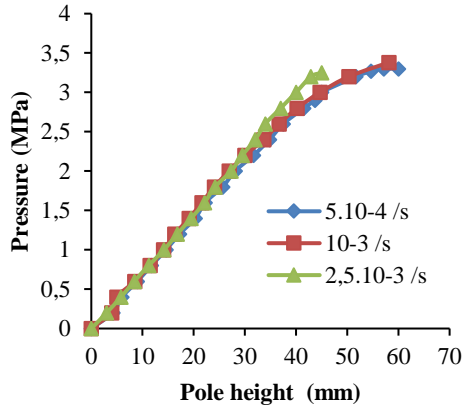


Fig. 9 Pressure as a function of height at the pole (T = 25°C): circular die (flow effect)

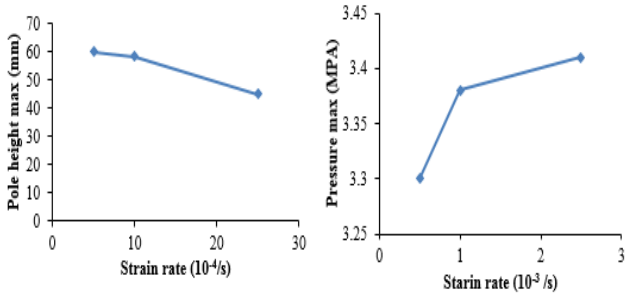


Fig. 10 Maximum pressure and height at the pole as a function of the average strain rate

decrease of 16% and a pressure increase of 3.3%. Refer to Fig. 10 for visual representation.

The measurement of the height at the pole is carried out by a digital calliper. The zero level of the measurement corresponds to the uncharged state of the specimen. The height at the pole is recorded at the centre of the active part for a given pressure. The measurement is carried out at the same time as the specimen is loaded. The tests representative of the variation of the pressure as a function of the height at the pole for the two circular and elliptical dies are made on circular specimens at different temperatures which vary from 25°C to 150°C and at different rolling directions (0°, 45°, 90°) to study the effect of anisotropy.

4.2. Effect of temperature on the formability of Aluminium 1050A

In this test, we need to study the effect of temperature on the sheet formability i.e. on the fracture zone and the height at the pole as well as on the pressure.

Through the different curves present in the four Figs. 12, 13, 14 and 15 we can say that the increase in temperature generates a decrease in the pressure applied to the sheet with an increase in displacement at break. Thus, it can be concluded that:

- the height at the pole increases from 80.33 mm at room temperature (25°C) to 89.35 mm at 100°C;
- the fracture zone changes during the forming process (Fig. 11), at ambient temperature, the rupture occurred at the pole of the spherical cap, at a temperature of 150°C, the fracture occurred at the plate-matrix contact edge;

- the pressure required to form the sheet decreases as the temperature increases.

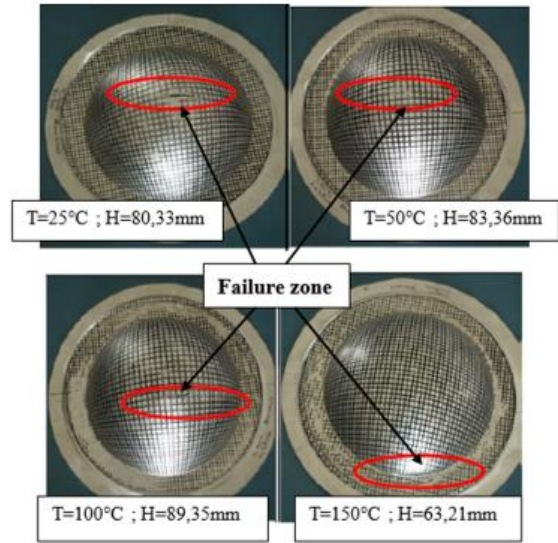


Fig. 11 Effect of temperature on the maximum displacement at the pole for circular die

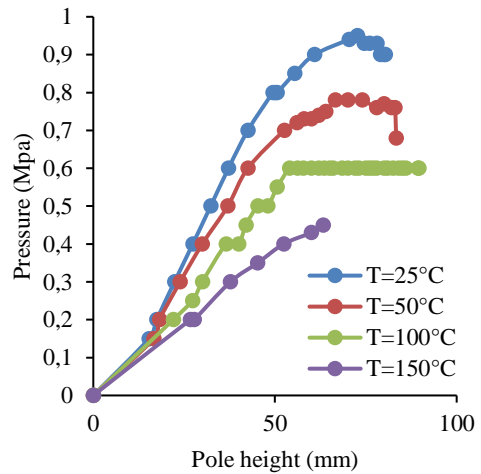


Fig. 12 Pressure as a function of height at the pole, circular die

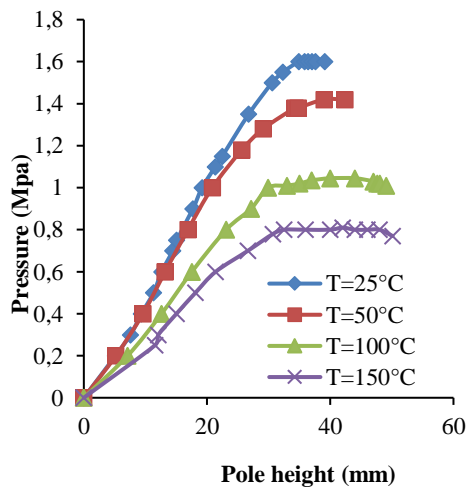


Fig. 13 Pressure as a function of height at the pole (90° direction), elliptical die

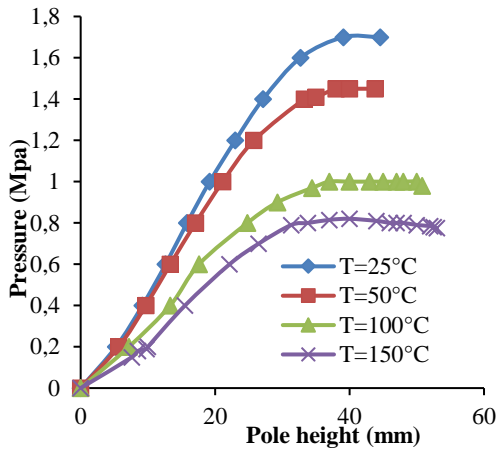


Fig. 14 Pressure as a function of the height at the pole (direction 45°), elliptical die

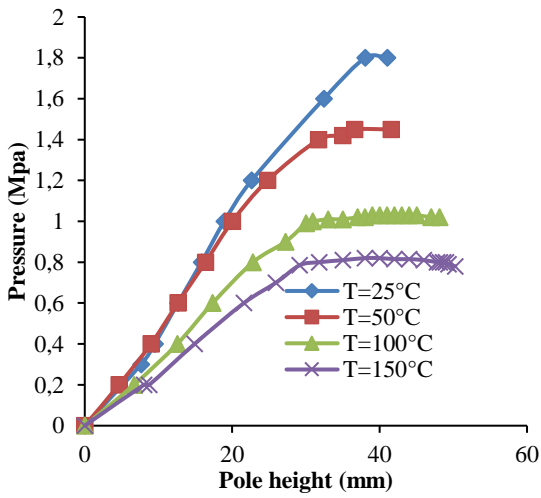


Fig. 15 Pressure as a function of the height at the pole (direction 0°), elliptical die

4.3. Effect of temperature on the anisotropy of aluminum 1050A

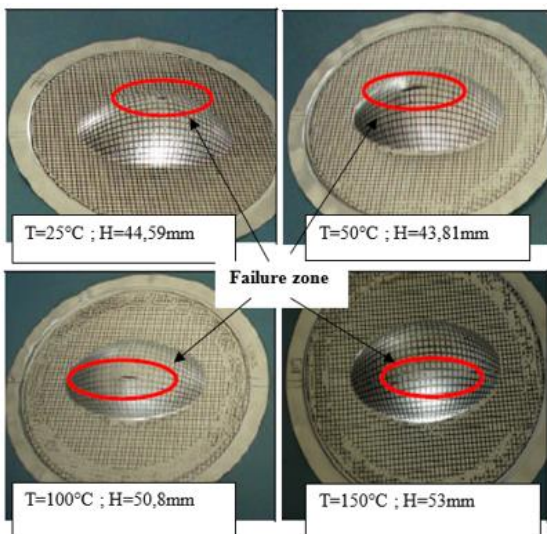


Fig. 16 Effect of temperature on the maximum displacement at the pole: elliptical die

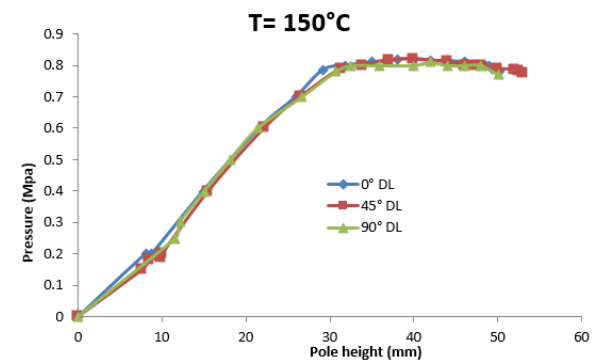
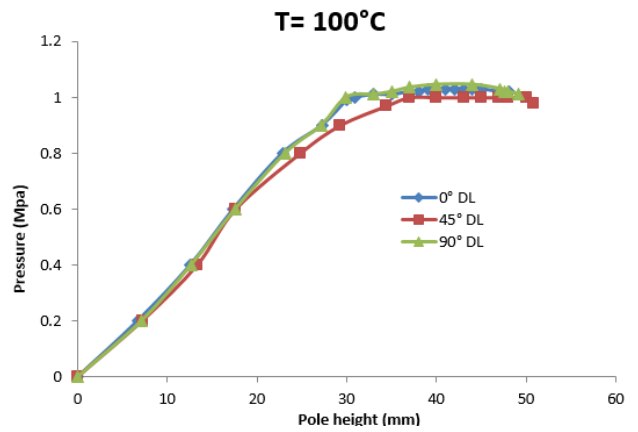
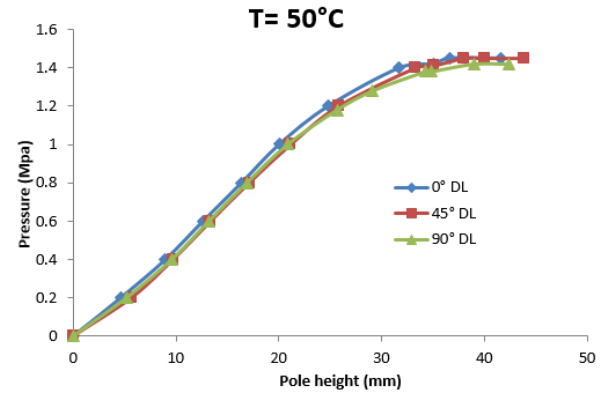
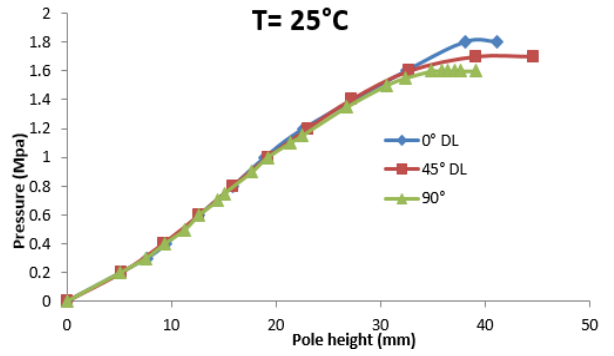


Fig. 17 Pressure as a function of height at the pole 25-150°C, elliptical die: 0°, 45° and 90°

Regarding the measurements obtained, Fig. 16 shows the change that follows the fracture zone during the forming process. At ambient temperature, the rupture oc-

curred at the pole of the spherical cap. Beyond ambient temperature, the rupture moved away from the pole to occur in regions increasingly close to the recessed edge of the blank.

Fig. 17 shows the variation of pressure versus pole height as a function of the variation of the orientation angle of the elliptical matrix at different temperatures. The curves are close for low pressure and move apart for breaking pressure, showing that the material is anisotropic.

The orientation of the elliptical matrix according to the three directions (0° , 45° and 90°) has a weak influence on the variation of the pressure according to the height at the pole. Table 1 summarizes the values of pressure and height at the pole for different orientations of the elliptical cavity matrix.

Oriented tensile tests were carried out to demonstrate the anisotropy of Al1050a (Fig. 19). The specimens used for the oriented tensile tests are prismatic in shape, with the dimensions defined in Fig. 18, and comply with French standard NF A 03-151.

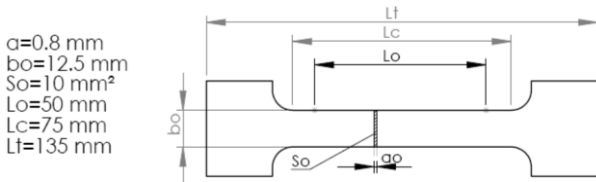


Fig. 18 Standard dimensions for tensile test specimens

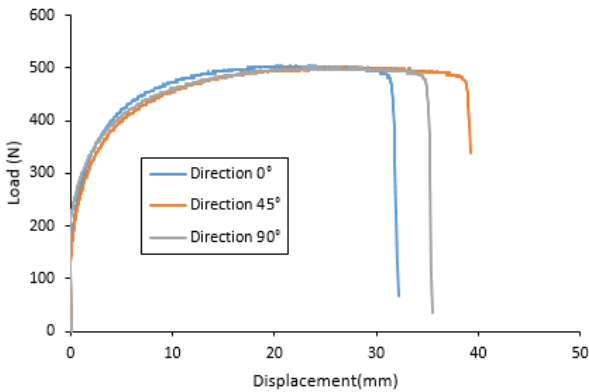


Fig. 19 Oriented tensile tests of Al1050a ($T = 25^\circ\text{C}$)

Table 1

Characteristics of aluminum 1050A for an elliptical die

Loading direction($^\circ$)	Maximum pressure, MPa	Maximum pole height, mm
0	1.8	38.07
45	1.7	39.1
90	1.6	34.88

5. Identification method

The objective is the identification of model of work hardening of Swift coupled with a variable of damage and the parameters of anisotropy of criterion of Hill48 giving a good concordance between the experimental response and the response obtained by EF.

* Circular die

The geometric model adopted is a thin circular plate with a diameter of 320mm and thickness of 0.8mm. It is meshed with eight-node hexahedral 3D solid elements (C3D8R) and comprises a total of 6552 elements in two

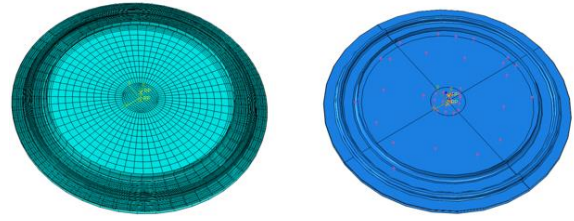


Fig. 20 Mesh size and boundary conditions of a bulge test specimen, circular die

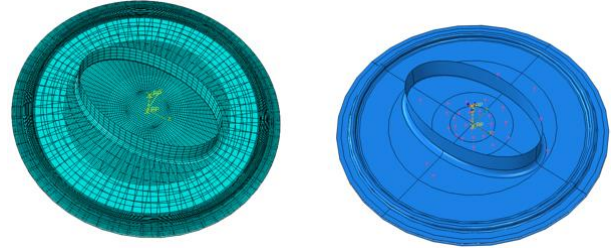


Fig. 21 Meshing and boundary conditions of a bulge test specimen: elliptical die

parts. The central part was meshed using a fine mesh, while the remaining part was meshed using a coarse mesh (Fig. 20). The circular die has an inside diameter of 220 mm and a fillet radius of 6mm. It is modeled by R3D4 shell elements, assumed to be rigid and undeformable. The Coulomb coefficient of friction between all solids in contact is 0.1.

Boundary conditions consist of an imposed embedding on the die and a linear pressure exerted on the blank, depending on the material to be tested.

* Elliptical die

The bulge test is identical to the previous case, except that the blank holder is elliptical, with a major axis of 170 mm and a minor axis of 102 mm (Fig. 21). The sheet mesh has 11992 C3D8R elements. The same boundary conditions used for the circular hold-down case are applied here. The general approach to achieve this is illustrated in Fig. 22.

The experimental data is in the form of a sample of points where the measurements were carried out (example: the height at the pole (h) for different values of pressure (p)). Numerically, the distance between the experimental curve and the simulated one was defined as the sum of the squares of the differences of the ordinates of the points of the same abscissa (the abscissas are imposed by the experimental points). The relative difference between the two curves is then defined by the relationship (17):

$$\xi_{r_0; r_{45}; r_{90}} = \left(\frac{1}{N} \sqrt{\sum_1^N \left(\frac{F_{i_{exp}} - F_{i_{num}} x}{F_{i_{exp}}} \right)^2} \right). \quad (17)$$

The reverse identification procedure to determine the parameters of the coupled Swift model and the Hill48 parameters was carried out according to the following steps:

- Step 1. We begin by identifying the uncoupled Swift model. One will determine the parameters of hardening K , ε_0 and n by considering $D = 0$.
- Step 2. We identify the parameters of the HILL load surface (F , G , H and N) representing the anisotropy of the

sheet, from the Bulge test with an elliptical blank clamp (direction 0°, 45° and 90° with respect to the rolling direction) by setting the work hardening parameters (K , ϵ_0 and n) to the values identified in step 1.

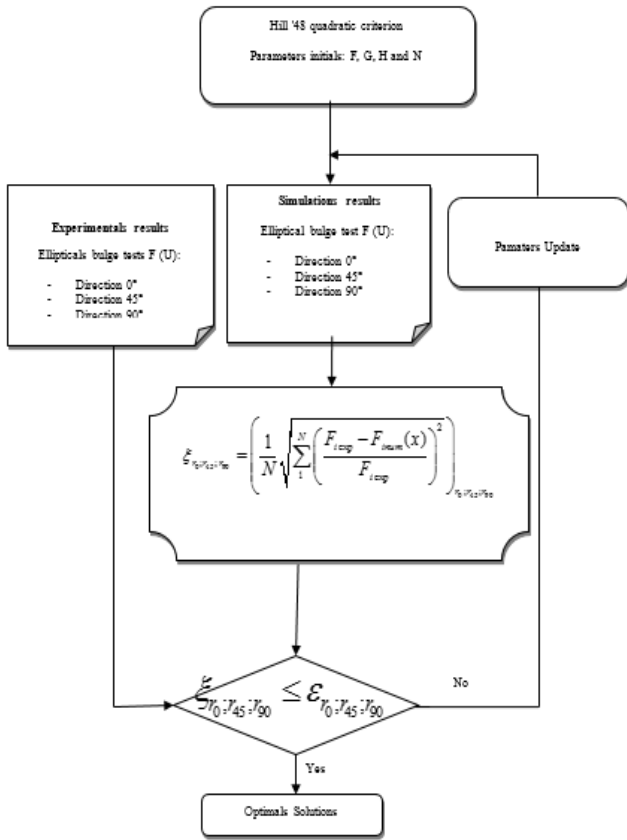


Fig. 22 Identification method of the anisotropic parameters

The identified strain hardening parameters are presented in Table 2. The height response at the pole as a function of the pressure is compared with the experimental response, for the case of a circular matrix, a good agreement has been observed (Fig. 23). The maximum relative difference is of the order of 2.9%.

To identify the material parameters at each temperature level, the calculations must be repeated in full according to the three steps.

Table 2 Results of the identification of work hardening parameters at different temperature levels of Aluminum 1050A

Temperature, °C	K , MPa	ϵ_0	n	Relative error ξ , %
25	216.9	0.009	0.38	2.9
50	112.826	0.01	0.228	0.6
100	95.375	0.01	0.226	1.2
150	73.827	0.01	0.215	2.4

The mechanical fields (equivalent stress and equivalent plastic strain) are illustrated in Fig. 24 for different temperature levels under isothermal condition. We note for a maximum displacement at the pole the maximum stress applied decreases with an increase in temperature of about 104.8 MPa at 25°C and 59.1 MPa at 150°C.

To further adjust the model, we adopted the same approach by going to step 2. This involves identifying the

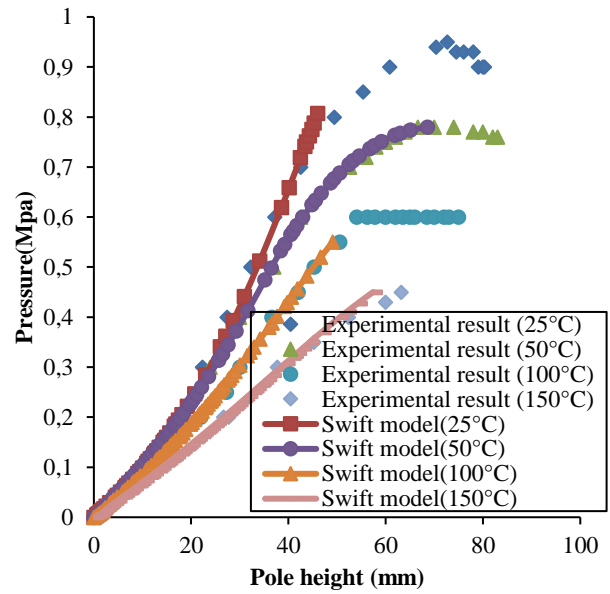


Fig. 23 Response curves height at the pole as a function of the pressure at different temperature levels hydraulic expansion test with circular clamp of aluminium 1050A

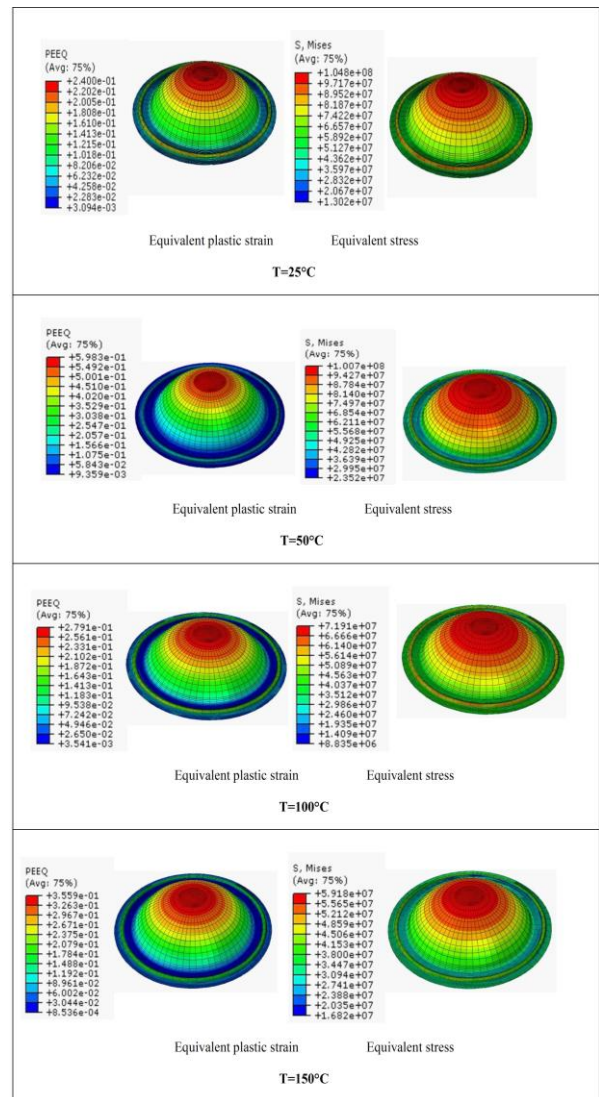


Fig. 24 Isovalues of equivalent stress and equivalent strain for annealed aluminium 1050A for a circular die (isothermal condition)

Lankford coefficients from the same type of test but in this case with an elliptical matrix since the latter puts highlight the importance of the anisotropy coefficients during blank deformation by changing the loading path. The parameters identified are presented in Table 3. For the case of an elliptical matrix at 25°C, good agreement was observed (Fig. 24). The maximum relative difference is around 3.46%.

Oriented tensile tests were used to identify the anisotropy parameters (Fig. 25). Fig. 26 shows the variation of the anisotropy parameters r_0 , r_{45} and r_{90} with respect to temperature. R values greater than 1.0 indicate good formability and resistance to thinning. As can be seen in Fig. 26, the values of r_0 and r_{45} increase with temperature, which indicates that the formability of aluminium sheet has improved also at high temperature.

In this step it is a question of identifying the parameters of the surface of load of HILL (F , G , H and N)

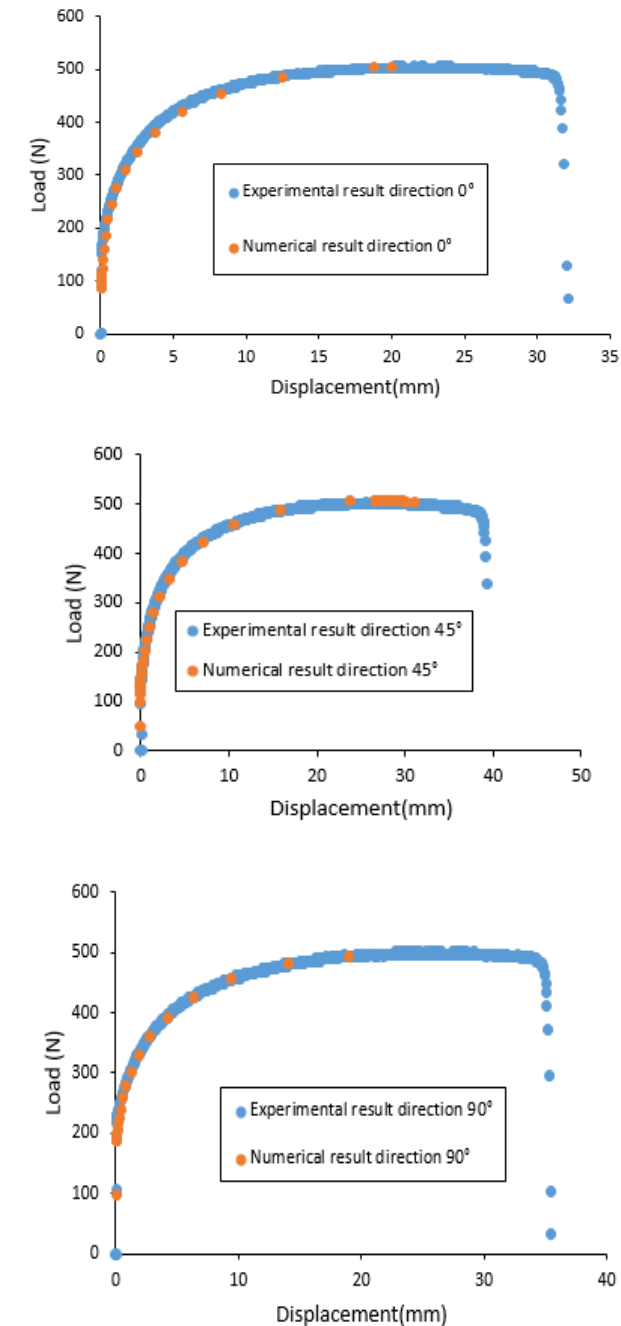


Fig. 25 Oriented tensile tests

Table 3

Results of the identification of Lankford coefficients at different temperature levels of Aluminum 1050A

Temperature (°C)	r_0	r_{45}	r_{90}	Relative error ξ (%)
25	1.45	0.5	2.1	3.41
50	1.501	0.719	1.878	3.46
100	1.898	1.088	0.733	2.98
150	2.249	1.333	0.653	3.2

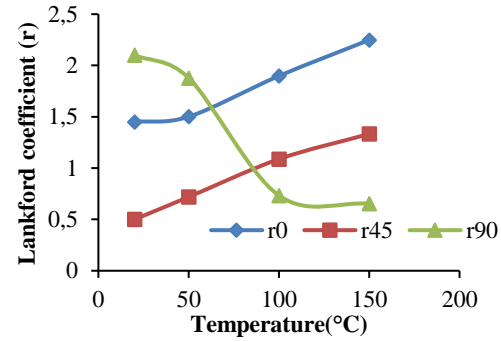


Fig. 26 Evolution of the Lankford coefficients of aluminium 1050A as a function of temperature

representing the anisotropy of the sheet are given according to the relation (2), (Fig. 27). Table 4 summarizes the identification results of the anisotropy parameters.

To study the influence of temperature on the anisotropy parameters, we constructed the charging surfaces for the different temperature levels. Fig. 28 shows the distortion suffered by the load surface as the temperature changes, this distortion corresponds to a rotation of a few degrees around the normal to the plane of the main axes, the rotation is accompanied by a decrease in the area of the surface considered.

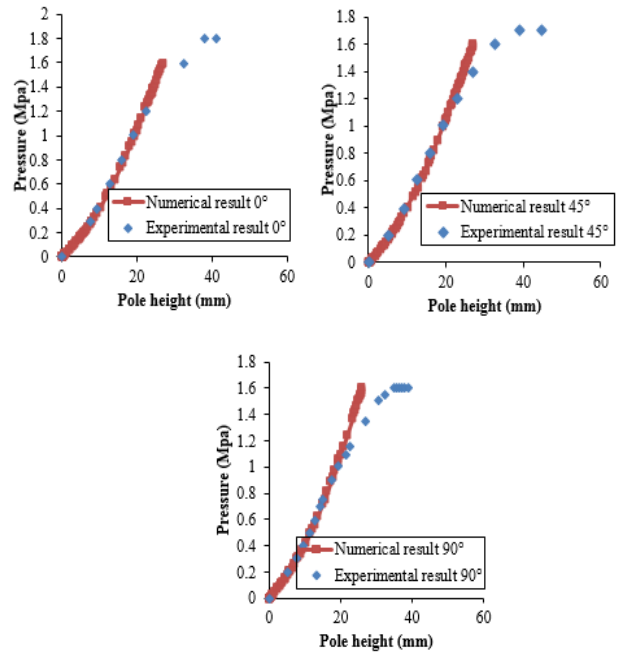


Fig. 27 Height response diagrams at the pole as a function of pressure at 25°C hydraulic expansion test with elliptical hold-down of aluminium 1050A

Table 4
Levels of anisotropy parameters of Hill48at different temperatures of Aluminum 1050a

Temperature, °C	<i>F</i>	<i>G</i>	<i>H</i>	<i>N</i>
25	0.281	0.408	0.591	1.126
50	0.319	0.399	0.6	1.275
100	0.893	0.345	0.654	2.729
150	1.06	0.307	0.692	3.491

The iso values of the equivalent stress and of the equivalent strain are given in Fig. 29 for a maximum displacement at the pole. It is noted that the equivalent stress in this zone decreases for an increase in temperature, at 25°C the stress is of the order of 123.2 MPa and at 150°C is of the order of 59.57 MPa. On the other hand, an increase in temperature generates an increase in the deformation equivalent to the pole, at 25°C the deformation is of the order of 0.21% and at 100°C it is equal to 0.42%.

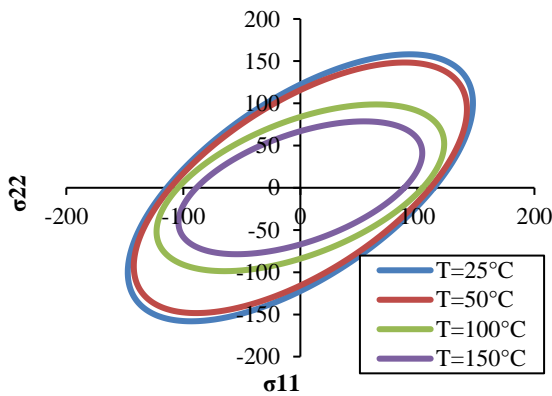


Fig. 28 Evolution of the Hill48 charging surface as a function of the temperature of the aluminium 1050A

6. Validation of the study of the anisotropy of aluminium 1050A

6.1. Diagram forming limit of the 1050A aluminum

The diagram forming limit for 1050A aluminum were calculated using two types of hardening laws: Swift's hardening law and the Hill48's plasticity criterion.

The Fig. 30 shows the forming limit curves for 1050A at different temperatures. As shown in this figure, the diagram forming limit increase with temperature, showing that 1050A can be stretched to higher levels to prevent failure from occurring.

6.2. Stamping test of the 1050A aluminum sheet

To validate the study of the plastic instability of aluminum 1050A, the results of the critical stresses were used to simulate an Erichsen-type stamping test. The objective of this study is to predict the failure zone of the sheet.

The Erichsen-type stamping test is a simple test used to study the ductility of metals. The punch descends on the sheet kept in contact until the blank cracks. The measured depth of drawing gives the Erichsen Index (EI).

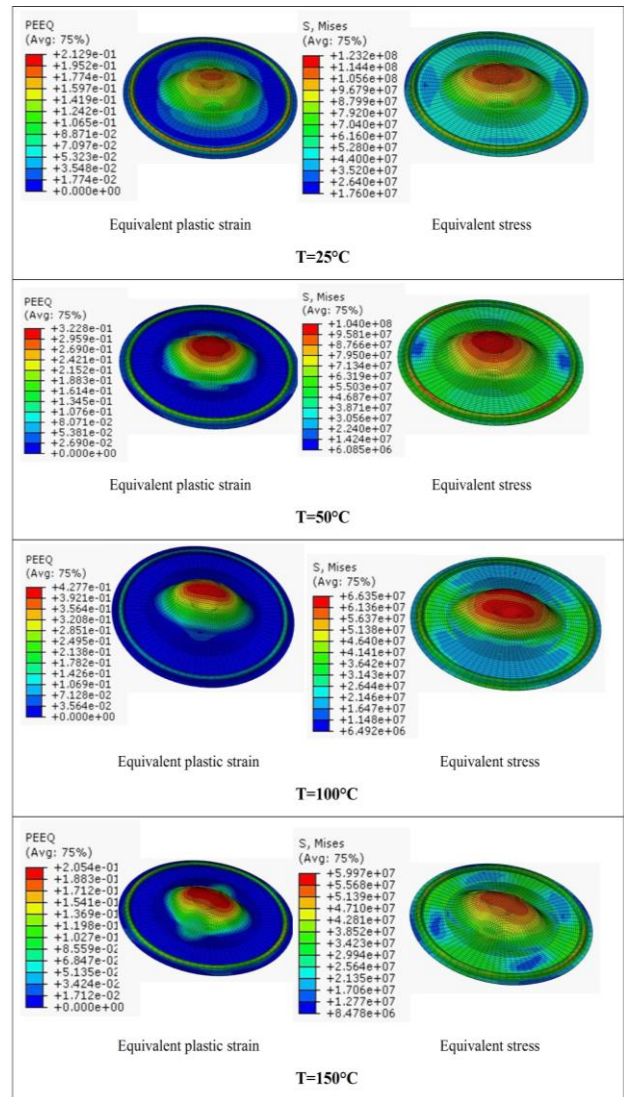


Fig. 29 Isovalues of the equivalent von Mises stress and of the equivalent plastic strain for aluminum 1050A for an elliptical blank-holder (direction 0°, isothermal condition)

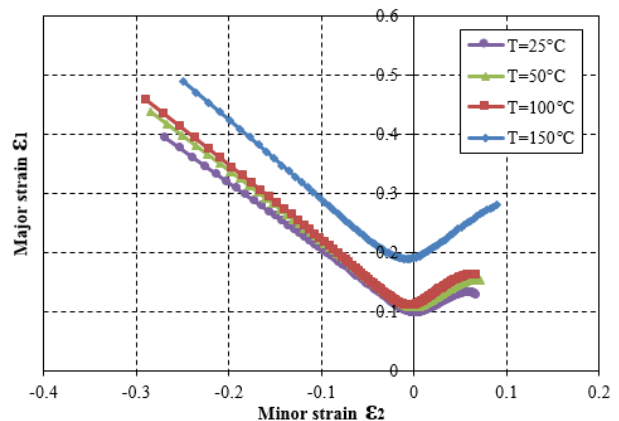


Fig. 30 Diagram forming limit as a function of the temperature of aluminium 1050A

The mesh of the sheet has 3202 elements of the C3D8R type (Fig. 31). The Coulomb coefficient of friction between all the solids in contact is equal to 0.1. The boundary conditions used are a normalized clamping force

of the blank clamp is equal to 10 kN and the degrees of freedom at the reference point of the die are blocked.

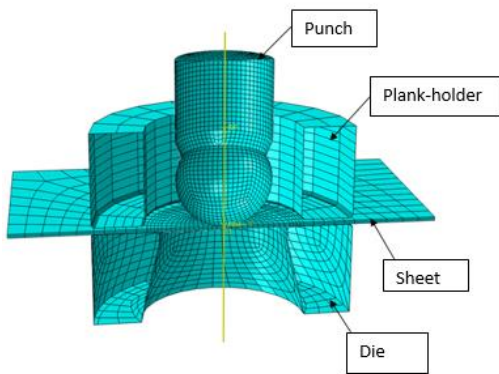


Fig. 31 Numerical modeling of an Erichsen-type stamping test

Figs. 32 and 33 show the validation results of the behaviour model parameter identification method. The identification results are very close to the experimental results.

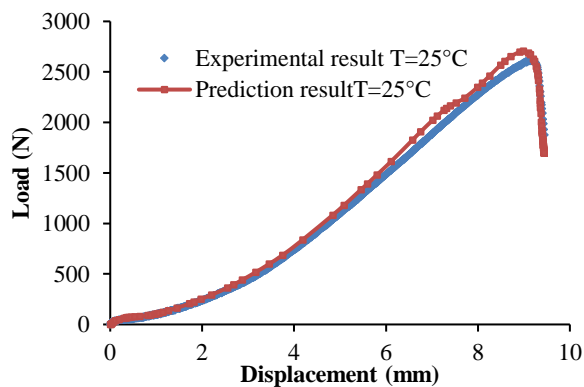


Fig. 32 Comparison between the experimental and numerical load/displacement results of the stamping test

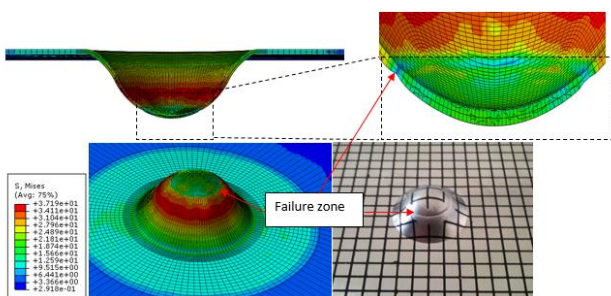


Fig. 33 Comparison between the experimental and numerical results of the stamping test: validation of the prediction of the failure zone

7. Conclusions

We have carried out experimental tests on hydroforming sheets with a circular and elliptical matrix, we study the influence of the parameters on the height at the pole (temperature, average speed of deformation, anisotropy, materials, etc.) and we validate the experimental results numerically using the law of work hardening SWIFT

and anisotropy Hill48 on ABAQUS for that it is necessary to follow an identification strategy to obtain a good concordance between the experimental and numerical approach.

The identification strategy that we are discussing is based on the choice of trials from which the behavior patterns will be identified. The objective is the identification of model of work hardening of Swift coupled with a variable of damage and the parameters of anisotropy of criterion of Hill48 giving a good concordance between the experimental response and the response obtained by EF. Tensile tests carried out on conventional standardized specimens at different orientations with respect to the rolling direction of the sheet, were used to characterize by a direct method, the anisotropy and work hardening of Al 1050A.

Acknowledgements

The authors gratefully acknowledge the approval and the support of this research study under the grant No. ENGA-2022-11-1941 from the Deanship of Scientific Research at Northern Border University, Arar, K.S.A.

References

1. **Delshad Gholami, M.; Hashemi, R.; Sedighi, M.** 2020. The effect of temperature on the mechanical properties and forming limit diagram of aluminum strips fabricated by accumulative roll bonding process, *Journal of Materials Research and Technology* 9(2): 1831-1846. <https://doi.org/10.1016/j.jmrt.2019.12.016>.
2. **Wang, Q.L.; Novella, M.F.; Ghiotti, A.; Bruschi, S.** 2017. Anisotropy influence on flow behaviour and plastic instability of Ti6Al4V sheets deformed in a wide range of temperatures and strain rates, *Procedia Engineering* 207: 2161-2166. <https://doi.org/10.1016/j.proeng.2017.10.975>.
3. **Goksen, S.; Darendeliler, H.** 2020. The Effect of Strain Rate and Temperature on Forming Limit Diagram for DKP-6112 and AZ31 Materials, 23rd International Conference on Material Forming (ESAFORM) 47: 1241-1244. <https://doi.org/10.1016/j.promfg.2020.04.194>.
4. **Chutwin Amree, Sansot Panich, Tanakorn Jantara-richa.** 2022. Polar effective plastic strain - forming limit diagram of DP 440 steel sheet with application to two-step forming test, *Materials Today: Proceedings*, <https://doi.org/10.1016/j.matpr.2022.11.385>.
5. **de Almeida, L.; Schön, C. G.** 2019. Evaluation of the formability of 90/10 brass produced by different casting processes and investigation of the effect of Forming Limit Diagram determination procedure, *Journal of Materials Research and Technology* 8(5): 4163-4172. <https://doi.org/10.1016/j.jmrt.2019.07.025>.
6. **Dheeraj, K.; Raj, M.D.; Singh, S.R.; Kishore, T.V.; Bandhavi, C.** 2022. Experimental determination of forming limit diagram for $\alpha+\beta$ brass at hot forming conditions, *Materials Today - Proceedings* 62(6): 4108-4116. <https://doi.org/10.1016/j.matpr.2022.04.657>.
7. **Rakshit, R.; Katiyar, B.S.; Tomé, C.N.; Panda, S.K.; Mandal, S.** 2023. A finite element coupled visco-plastic self-consistent simulation to predict micro-texture and anisotropy evolution during single point incremental

- forming in Al-Li alloy, *Journal of Materials Processing Technology* 312: 117834.
<https://doi.org/10.1016/j.jmatprotec.2022.117834>.
8. **Cauvin, L.; Raghavan, B.; Jin, J.Q.; Bouvier, S.; Wang, X.D.; Meraghni, F.; Alves, J.L.** 2022. Investigating the plastic anisotropy and hardening behavior of a commercial Zn–Cu–Ti alloy: Experimental & modeling approach, *Mechanics of Materials* 164: 104103.
<https://doi.org/10.1016/j.mechmat.2021.104103>.
 9. **Chatti, M.; Gratton, M.; Caliez, M.; Frachon, A.; Picart, D.; Hocine, N.A.** 2022. Experimental investigation of the behaviour of a simulant material for plastic-bonded explosives and modelling of the effectivity and damage induced anisotropy, *Mechanics of Materials* 172: 104388.
<https://doi.org/10.1016/j.mechmat.2022.104388>.
 10. **Paux, J.; Ben Bettaieb, M.; Badreddine, H.; Abed-Meraim, F.; Labergere, C.; Saanouni, K.** 2021. An advanced elastoplastic framework accounting for induced plastic anisotropy fully coupled with ductile damage, *International Journal of Mechanical Sciences* 207: 106620.
<https://doi.org/10.1016/j.ijmecsci.2021.106620>.
 11. **Hou, Y.; Du, K.; Abd El-Aty, A.; Lee, M.-G.; Min, J.** 2022. Plastic anisotropy of sheet metals under plane strain loading: A novel non-associated constitutive model based on fourth-order polynomial functions, *Materials & Design* 223: 111187.
<https://doi.org/10.1016/j.matdes.2022.111187>.
 12. **Song, J.; Zhou, H.; Xu, Y.M.; Jiang, W.; Zhang, C.W.** 2022. Molecular dynamics simulation and experimental investigation on deformation anisotropy of gallium nitride Ga-plane and N-plane nano-scratching, *Solid State Communications* 353: 114866.
<https://doi.org/10.1016/j.ssc.2022.114866>.
 13. **Saxena, R.; Narayanan, R.G.; Robi P.S.** 2021. Performance evaluation of stamping lubricants during elevated temperature forming of SS304 sheets using forming limit diagram, *Materials Today - Proceedings* 44(1): 1761-1764.
<https://doi.org/10.1016/j.matpr.2020.11.958>.
 14. **Liu, B.S.; Cao, F.; Zeng, Y.; Wu, W.** 2022. Numerical and experimental study on temperature and springback control of U-shape titanium extrusion hot stretch bending, *International Journal of Lightweight Materials and Manufacture* 5(4): 453-469.
<https://doi.org/10.1016/j.ijlmm.2022.05.007>.
 15. **Ridha, H.; Almitani, K.H.; Chamekh, A.; Toumi, H.; Tavares, J.M.R.S.** 2015. A theory for bone resorption based on the local rupture of osteocytes cells connections: A finite element study, *Mathematical Biosciences* 262: 46-55.
<https://doi.org/10.1016/j.mbs.2015.01.005>.
 16. **Gras, T.; Hamdi, M.-A.; Ben Tahar, M.; Tanneau, O.; Beaubatie, L.** 2018. On a coupling between the Finite Element (FE) and the Wave Finite Element (WFE) method to study the effect of a local heterogeneity within a railway track, *Journal of Sound and Vibration* 429: 45-62.
<https://doi.org/10.1016/j.jsv.2018.05.011>.
 17. **Benzarti, Z.; Khalfallah, A.; Bougrioua, Z.; Evaristo, M.; Cavaleiro, A.** 2023. Understanding the influence of physical properties on the mechanical characteristics of Mg-doped GaN thin films, *Materials Chemistry and Physics* 307: 128182.
<https://doi.org/10.1016/j.matchemphys.2023.128182>.
 18. **Hill, R.** 1990. Constitutive modelling of orthotropic plasticity in sheet metals, *Journal of the Mechanics and Physics of Solids* 38(3): 405-417.
[https://doi.org/10.1016/0022-5096\(90\)90006-P](https://doi.org/10.1016/0022-5096(90)90006-P).
 19. **Leacock, A.G.** 2006. A mathematical description of orthotropy in sheet metals, *Journal of the Mechanics and Physics of Solids* 54(2): 425-444.
<https://doi.org/10.1016/j.jmps.2005.08.008>.
 20. **Barlat, F.; Lege, D.J.; Brem, J.C.** 1991. A six-component yield function for anisotropic materials, *International Journal of Plasticity* 7(7): 693-712.
[https://doi.org/10.1016/0749-6419\(91\)90052-Z](https://doi.org/10.1016/0749-6419(91)90052-Z).
 21. **Barlat, F.; Maeda, Y.; Chung, K.; Yanagawa, M.; Brem, J.C.; Hayashida, Y.; Lege, D.J.; Matsui, K.; Murtha, S.J.; Hattori, S.; Becker, R.C.; Makosey, S.** 1997. Yield function development for aluminium alloy sheets, *Journal of the Mechanics and Physics of Solids* 45(11-12): 1727-1763.
[https://doi.org/10.1016/S0022-5096\(97\)00034-3](https://doi.org/10.1016/S0022-5096(97)00034-3).
 22. **Banabic, D.; Kuwabara, T.; Balan, T.; Comsa, D.S.** 2004. An anisotropic yield criterion for sheet metals? *Journal of Materials Processing Technology* 157-158: 462-465.
<https://doi.org/10.1016/j.jmatprotec.2004.07.106>.
 23. **Li, H.; Zhang, L.W.; Chen, G.Y.; Ma, J.; Wei, D.; Bian, T.J.; Yang, J.C. Wu, C.H.; Yang, H.** 2022. Time-dependent springback of high strength titanium tubular materials: Experiment and modeling, *Journal of Materials Processing Technology* 299: 117354.
<https://doi.org/10.1016/j.jmatprotec.2021.117354>.
 24. **Nasri, M.T.; Abbassi, F.; Ahmad, F.; Makhoulfi, W.; Ayadi, M.; Mehboob, H.; Choi, H.S.** 2022. Experimental and numerical investigation of sheet metal failure based on Johnson-Cook model and Erichsen test over a wide range of temperatures, *Mechanics of Advanced Materials and Structures* 30(10): 2087-2100.
<https://doi.org/10.1080/15376494.2022.2049934>.
 25. **Kim, J.; Kim, S.W.; Song, W.J.; Kang, B.S.** 2004. Analytical approach to bursting in tube hydroforming using diffuse plastic instability, *International Journal of Mechanical Sciences* 46(10): 1535-1547.
<https://doi.org/10.1016/j.ijmecsci.2004.09.001>.
- A. Eladeb, M. T. Nasri, N. Becheikh, N. Ghazouani, M. A. Tashkandi
- STUDY ON THE THERMAL SENSITIVITY OF ANISOTROPIC THIN SHEETS: APPLICATION TO HOT BULGE TESTS
- S u m m a r y
- This article presents a study on the thermal sensitivity of anisotropic thin sheets, focusing specifically on their behavior during hot bulge tests. Anisotropic materials exhibit different mechanical properties in different directions, and understanding their response to thermal loading is crucial for various engineering applications.
- The experimental investigation involves subjecting thin sheets of anisotropic materials to controlled thermal

conditions and measuring their response. The hot bulge test, a well-established method, is employed to analyze the behavior of the sheets under elevated temperatures. This test involves applying a controlled internal pressure to a heated circular and elliptical specimen, causing it to deform and form a bulge.

Through this study, the thermal sensitivity of anisotropic thin sheets is characterized by analyzing the bulge height, bulge profile, and strain distribution. The influence of various factors, such as temperature, material anisotropy, and loading rate, is examined to understand their effects on the sheet's response.

Experimental results reveal significant variations in the thermal sensitivity of anisotropic thin sheets, depending on the material's orientation and temperature. The study demonstrates that certain orientations exhibit greater sensitivity to thermal loading, leading to distinct bulge profiles and strain distributions.

Furthermore, numerical simulations are conducted using finite element analysis to validate and complement the

experimental findings. The simulation models incorporate the anisotropic material properties and the thermal boundary conditions, enabling a comprehensive understanding of the thermal sensitivity behavior observed experimentally.

The outcomes of this study provide valuable insights into the thermal behavior of anisotropic thin sheets, particularly in the context of hot bulge tests. The findings contribute to the knowledge base of material characterization and can aid in the design and optimization of structures and components subjected to thermal loading, where anisotropic materials are involved.

Keywords: thermal sensitivity, anisotropic materials, thin sheets, hot bulge tests, mechanical properties, finite element analysis.

Received May 28, 2023

Accepted April 15, 2024



This article is an Open Access article distributed under the terms and conditions of the Creative Commons Attribution 4.0 (CC BY 4.0) License (<http://creativecommons.org/licenses/by/4.0/>).